Structures of [M(Ura-H)(H2O)n]+ (M = Mg, Ca, Sr, Ba; n = 1–3) complexes in the gas phase by IRMPD spectroscopy and theoretical studies

Barry Power, Violette Haldys, Jean-Yves Salpin, Travis D Fridgen

Structures of $[M(Ura\text{-}H)(H_2O)_n]^+$ (M=Mg, Ca, Sr, Ba; n=1–3) complexes in the gas phase by IRMPD spectroscopy and theoretical studies

Barry Power,[a] Violette Haldys,[b,c] Jean-Yves Salpin,[b,c] and Travis D. Fridgen[a]

a: Department of Chemistry, Memorial University, St. John's, NL, A1B 3X7, Canada.

b: Université

d'Evry Val d'Essonne – Laboratoire d'Analyse et Modélisation pour la Biologie et l'Environnement (LAMBE) –Bâtiment Maupertuis, Boulevard François Mitterrand, 91025 Evry, Francec : CNRS UMR 8587

Abstract

The structures of singly and doubly (and for Mg, triply) hydrated group 2 metal dications bound to deprotonated uracil were explored in the gas phase using infrared multiple photon dissociation (IRMPD) spectroscopy in the mid-infrared region (1000–1900 cm^{-1}) and the O-H/N-H stretching region (2700–3800 cm^{-1}) in a Fourier transform ion cyclotron resonance mass spectrometer (FTICR-MS). The IRMPD spectra were then compared to the computed IR spectra for various isomers. Calculations were performed using B3LYP with the 6-31+G(d,p) basis set for all atoms except Ba^{2+} and Sr^{2+}, for which the LANL2DZ or the def2-TZVPP basis sets with relativistic core potentials were used. Atoms-in-molecules (AIM) analysis was conducted for all lowest energy structures. The lowest energy isomers in all cases are those in which the one uracil is deprotonated at the N3 position and the metal is coordinated to the N3 and O4 of uracil. Regardless of the degree of solvation, all water molecules are bound to the metal ion and participate in a hydrogen bond with a carbonyl of the uracil moiety.

1. Introduction

Independently, both metal ions and solvents, notably water, have been thoroughly investigated for the roles they play in biological systems. In particular, the influence each holds on the behaviour of DNA and RNA nucleobases have been of great interest. In the case of metal dications, it has been shown that they are crucial for the stability of DNA and RNA through charge neutralization and noncovalent interactions with the phosphate backbone of the nucleic acids [1–3]. However, when in an undesirable excess, the metal dications may also change the conformation of the individual nucleobases away from the preferred canonical form, leading to deviations from the predicted Watson-Crick pairings through modification of hydrogen bonding sites [4–7]. These unwanted conformational changes can lead to genetic defects.

When uracil is in aqueous solution, the conjugate bases resulting from the loss of both N1 and N3 protons exist in equilibrium with a pK_a measured to be 9.5 [8]. However, in the gas phase, the acidity of both sites are dramatically different. Loss of the proton at N3 is associated with a deprotonation enthalpy of 1452 ± 17 kJ mol^{-1} [9], whereas to deprotonate at N1 requires 1393 ± 17 kJ mol^{-1} [9,10]. Various calculation methods [10–12] are in agreement on these thermochemical values. To resolve the differences between the gas and solvent phase values, Bachrach and Dzierlenga [13] employed microsolvation to model this solvent effect using DFT methods, and determine at what point bulk solvent effects become prevalent. It was determined that the gap in deprotonation energy decreases successively with each water molecule added up to the fourth water, at which point the gap in deprotonation energy has halved. Addition of a fifth and sixth water molecule have a negligible effect on the difference between deprotonation energies.

The focus of this current work is to examine the RNA nucleobase uracil, and the complexes formed with group 2 metal dications at varying degrees of water solvation. The conventional uracil numbering scheme used throughout is presented in Scheme 1. Though the deprotonation energy at the N1 site of uracil is lower in the gas phase compared to N3, previous studies have all concluded that deprotonation occurs at N3 in the presence of alkaline earth metal cations [14,15,16], or heavy metals (REF : add Guillaumont et al. IJMS, v243,p279-293 (2005)). Of course, replicating the cellular environment in condensed phase analysis is difficult. To overcome this, gas-phase conditions are utilized, allowing for direct molecular examination and eliminating the interference of bulk solvent effects, which may otherwise influence the structure of such complexes. Action, or consequence spectroscopy, is a method that has successfully been applied to conduct such research. In particular, infrared multiple photon dissociation (IRMPD) is a technique frequently used and is the method of choice for this current work [17,18].

The current work aims to provide structural insight into the hydrated alkaline earth metal complexes, $[M(Ura\text{-}H)(H_2O)_n]^+$ (M = Mg, Ca, Sr, Ba), using IRMPD spectroscopy in both the O-H/N-H stretching region (2700–3800 cm^{-1}) as well as the fingerprint region (1000–1900 cm^{-1}). In this fingerprint region, carbonyl stretching frequencies are obtained and differentiating features between the computed tautomers, previously indistinguishable, are now evident.

2. Methods

2.1. Experimental. All mid-infrared experiments were performed using a Fourier-transform ion cyclotron resonance mass spectrometer (FT-ICR-MS) coupled to a mid-infrared free electron laser (FEL) at the Centre Laser Infrarouge d'Orsay (CLIO) [19,20]. 0.01 mmol L^{-1} solutions of the chloride salts of each of the metal ions and 1 mmol L^{-1} uracil solutions were prepared in 18 MΩ

water (Millipore). Mixtures were then prepared in a 1 to 10 ratio of metal solution to uracil solution, and introduced *via* syringe injection to the electrospray ion source at a flow rate of 75 μL/h. Ions were mass selected with a quadrupole mass filter, isolated in the ICR cell, and irradiated with the free electron laser. To accomplish hydration of the ions, the bare $[M(Ura-H)]^+$ ion was first selected in the quadrupole filter and then stored in the hexapole storage cell, into which water vapour had been leaked [21]. Irradiation times varied from 0.1 to 3 seconds, with the more weakly bound and, therefore, faster dissociating ions being irradiated for the shortest time. Certain areas of the IRMPD spectra which were saturated were scanned after attenuation of the FEL. The laser was scanned at 5 cm^{-1} intervals from ~1000 to 1900 cm^{-1}.

Experiments in the O-H/N-H region were conducted at the Laboratory for the Study of the Energetics, Structures, and Reactions of Gaseous Ions at Memorial University using a Bruker Apex Qe 7T Fourier-transform ion cyclotron resonance mass spectrometer coupled with an IR OPO tunable laser as previously described [22]. Solutions were prepared to 1mM of both uracil and metal ion in a 50:50 methanol-water solvent system. The solutions were syringe injected into the electrospray ion source at a flow rate of 160 μL/h. The ions emerging from the source were mass-selected using a quadrupole mass filter, accumulated in the hexapole collision cell, then guided into the ICR cell. The ions were then irradiated with tunable infrared radiation in the O-H/N-H stretching region from 2700 to 3800 cm^{-1} at an irradiation time between 1.5 and 3 seconds. The laser was scanned in 2 cm^{-1} intervals to yield the IRMPD spectra.

The IRMPD efficiency is the negative of the natural logarithm of parent ion intensity divided by the sum of parent and fragment ion signals.

2.2. Computational. Calculations for all structures were conducted using the Gaussian 09 suite of programs [23]. Each structure was optimized and infrared spectra computed using B3LYP density functional theory. In the cases of the Ca^{2+} and Mg^{2+} complexes, the 6-31+G(d,p) basis set was used for all atoms. For the complexes of Ba^{2+} and Sr^{2+}, the LANL2DZ basis set with relativistic core potential was used for strontium and barium atoms and the 6-31+G(d,p) basis was used for all other atoms. Single point energy calculations were then carried out using B3LYP with the 6-311+G(3df,3pd) basis set on all atoms except Sr and Ba, for which the LANL2DZ basis set with relativistic core potential was used. This computational method will be referred to as method 1.

All calculations were then repeated with the def2-TZVPP basis set, which has been found to work better for metal-cation amino acid complexes than the LANL2DZ [24,25], for all metal atoms during both the optimization and single point energy calculations. The 6-31+G(d,p) basis set was again used for all other atoms (C, H, N and O) during optimization, followed by the 6-311+G(3df,3pd) basis set for single point energy calculations. This computational method will be referred to as method 2.

These single-point electronic energies, using methods 1 and 2 were used to compute the enthalpies and Gibbs energies of isomeric species at 298K, using the unscaled harmonic vibrational frequencies calculated for optimization geometry.

The bonding within the individual equilibrium structures was also analyzed by locating the bond critical points (BCPs) using atoms-in-molecules (AIM) theory [26], which is based on a topological analysis of the electronic density at the BCPs, and is a good descriptor of the bond strength or weakness. This analysis was conducted using AIMAll software [27] with the optimized structures from method 2. Data from the topological analysis are given collectively in the Supporting Information as Figure S20.

For comparison with the experimental spectra, the computed infrared spectra were scaled by a factor of 0.97 in the fingerprint region, by 0.96 in the O-H/N-H region, and convoluted with a Lorentzian profile with a width (FWHM) of 15 cm^{-1}.

3. Results and Discussion

3.1. Examination of the IRMPD spectra. When complexes were irradiated by both the FEL and OPO, regardless of the metal or the degree of hydration, only water molecules were lost upon irradiation. This is in agreement with the loss of water molecule in the singly-hydrated complexes involving either Ba, Sr, or Pb and two uracil units, where only the loss of water was observed [14,28]. In these studies, only loss of a single water molecule is noted for the doubly-hydrated dimer complexes, whereas in the current work sequential dehydration corresponding to the losses of one and/or two water molecules is observed.

Figure 1 presents the IRMPD spectra for $[M(Ura\text{-}H)(H_2O)]^+$ in the 1000–1900 cm^{-1} region. All $[M(Ura\text{-}H)(H_2O)]^+$ spectra display a broad band centered between 1612 and 1620 cm^{-1}, which contains a combination of stretching modes; hydrogen-bonded C=O stretching, H_2O scissoring and C5=C6 stretching. This band is red-shifted with respect to the position of the free carbonyl stretch of uracil, centered about 1750 cm^{-1} in the gas phase [29], presumably due to hydrogen bonding which has the effect of lengthening and weakening the carbonyl bond. Both the H_2O scissoring mode and the C=C stretch also occur int this region, with the C=C stretch in particular being previously observed at the same frequency in similar complexes [15**Erreur ! Signet non défini.**].

Another intense band for all $[M(Ura\text{-}H)(H_2O)]^+$ complexes is centered around 1510–1527 cm^{-1}. This band is attributed to the metal-coordinated carbonyl stretch. Again this band is red-

shifted compared to the free carbonyl stretch of uracil which occurs about 1750 cm^{-1} as previously mentioned [29]. It is also a significant red-shift in comparison to the sodium-coordinated carbonyl stretch in uracil, observed to absorb between 1630 cm^{-1} and 1675 cm^{-1} [30], as well as the uracil dimers of these same metal ions, where the corresponding absorptions were found between 1614 cm^{-1} and 1627 cm^{-1}, depending on the metal [15]. In fact, the observed frequencies in the present work correspond more closely to the enol stretches in the dimer complexes, which absorbed between 1530 cm^{-1} and 1548 cm^{-1}, an indication that the carbonyl bond is significantly weakened in these monomeric complexes when compared to the dimers. The carbonyl weakening in the present monomeric complexes is due to the fact that the metal ion is now coordinated to a single carbonyl, instead of two.

Weaker features are visible at approximately 1400 cm^{-1} and 1200 cm^{-1} for the complexes of Ba, Sr and Ca. The broad band around 1400 cm^{-1} contains C-N stretches within the uracil ring, as well as the N1 hydrogen wagging vibration. At 1200 cm^{-1}, the C5 and C6 hydrogen wagging modes occur.

The IRMPD spectra in the fingerprint region of $[M(Ura-H)(Ura)(H_2O)_2]^+$ complexes are shown in Figure 2. The doubly-hydrated Mg complex could not be isolated during these particular experiments, although a spectrum was obtained in the O-H/N-H region. The spectra are consistent with the singly-hydrated complexes, however the narrowing and a slight blue-shift (~10 cm^{-1}) of the major feature is presently observed. However, the same modes are predicted to be contained in the band (hydrogen bonded carbonyl stretching, H_2O scissoring and C5=C6 stretching). The secondary feature, now detected between 1481 and 1527 cm^{-1}, once again is indicative of the metal-coordinated carbonyl stretching mode. This band noticeably blue-shifts as the metal decreases in size.

Even though the doubly-hydrated Mg complex could not be isolated in enough abundance to be examined during the experiments at CLIO, the triply-hydrated complex was easily detected. The IRMPD spectrum for $[Mg(Ura-H)(H_2O)_3]^+$ is presented in Figure 2 (top). There is now some distinction made between the stretches occurring between 1580 and 1680 cm^{-1}. The main band centered about 1622 cm^{-1} is now much narrower than it was for the singly and doubly-hydrated species. The carbonyl stretch at the O2 position has been blue-shifted to 1680 cm^{-1} and is now separated from the predominant band, which contains the scissoring stretch of the water molecule hydrogen-bonded to O2, as well as the C5=C6 stretch. Both synchronous and asynchronous scissoring of the other water molecules hydrogen bonded to O4 appear as a shoulder on the red side of the main band. The secondary carbonyl stretching feature, the metal-coordinated carbonyl, is also blue-shifted in comparison to the singly and doubly-hydrated species, to 1538 cm^{-1}. Blue shifting of carbonyl stretches has been previously observed upon hydration of these types of complexes [15]. The effect is likely the result of water binding to the metal, thus donating electron density back to the complex, and particularly to the carbonyl bonds. This leads to a mild strengthening of the C=O bond, and in turn, a higher stretching frequency.

Figure 3 presents the experimental spectra of the hydrated complexes of Ca and Mg in the O-H/N-H stretching region. Similar complexes of Ba and Sr have been examined previously [14]. All spectra exhibit the same key features. First, a band centered 3455 cm^{-1} for the singly-hydrated complexes, which gradually blue-shifts with increasing hydration, indicative of the N-H stretch of uracil. Secondly, the free O-H stretching modes of water, located in the range of 3600-3700 cm^{-1}. As the degree of hydration increases, more of these stretches are logically observed. In the singly-hydrated complexes, there is a single free O-H stretching mode, however as more water molecules added, symmetric and asymmetric modes are also observed.

3.2. Computed structures for [M(Ura-H)(H_2O)]$^+$. A total of 7 isomers were located for the singly-hydrated complexes of all metals. Figure 4 gives the structures and energetics for the three lowest energy structures. All structures obtained for both calculation methods are given in Figures S1 to S8 along with the thermochemistries, while Table S1 compares the relative energies obtained with both calculations methods. In all instances, the N3O4/wbO2 isomer is the most stable form in relative enthalpy. It is also the global minimum in relative Gibbs free energy (298 K) for all complexes, excepting for the the Mg complex, for which the N3O4/w structure is the global minimum. This result is identical to previous results obtained for the complexes of Ba and Sr [14]. This particular N3O4/w structure is deprotonated at the N3 of uracil, with metal coordination between N3 and O4. In addition, the water molecule is oriented away from the uracil moiety and does not interact with uracil.

For N3O4/wbO2 forms, the AIM topological analysis confirms the bidentate interaction, with two bond critical points (BCPs) connecting the metal to uracil in all complexes, and with corresponding positive values of the Laplacian of the electron density, $\nabla^2\rho$, suggesting electrostatic interactions (Supporting Information Fig. S20). Water is bound to the metal center, with an intramolecular hydrogen bond formed between the water and O2 of uracil, which is also confirmed through AIM analysis. The hydrogen bond is particularly strong for the Ba, Sr and Ca complexes, measuring ~1.6Å for each, with the hydrogen bond length increasing (and thus, decreasing in strength) with decreasing the metal ion size. For the Mg complex, the hydrogen bond length is 1.942 Å. This is similar to the results observed for water-carbonyl hydrogen bond in metal-uracil dimers [15], although the hydrogen bonds were much stronger in the case of the monomers. The carbonyl bond lengths vary, with the hydrogen-bonded carbonyl slightly shorter (~1.24 Å) than the metal

coordinated carbonyl bond length (1.28 Å). Distinct patterns are observed based on the size of the metal. As the metal size increases, the metal-coordinated carbonyl bond lengths decrease slightly, an expected result based upon decreasing metal-carbonyl bond strengths and confirmed by the computed electron densities at the BCPs. The increasing metal size also leads to the lengthening of the hydrogen-bonded carbonyl groups.

For the complexes of Ba, Sr and Ca, only one other form comes relatively close in terms of energy. In the N3O2/wbO4 conformation, uracil is again deprotonated at the N3 position. However, metal coordination now occurs between N3 and O2, with the water molecule coordinated to the metal center and hydrogen-bonded to the O4 position. For these metals, the difference in enthalpy and Gibbs free energy between these two structures is between 5.8 and 7.1 kJ mol^{-1}. All other structures were found to be significantly higher in energy, using both calculation methods, by at least 23 kJ mol^{-1}. For the complex of Mg, the N3O4/wbO2 structure is, like the other metals, lowest in enthalpy. However, the structure which is lowest in Gibbs free energy (N3O4/w), was deemed as an insignificant contributor for the other metal complexes. ~~The N3O4/w structure is consistent in deprotonation of uracil at N3. The Mg is coordinated between N3 and O4, and water is coordinated to Mg. However, the water molecule is oriented away from the uracil moiety and has no interaction with the uracil.~~

To conclude, all lowest energy structures exhibit planar geometry, regardless of calculation method.

3.2.1. Comparison of computed and experimental spectra. A comparison between the experimental spectra and the three lowest energy structures computed *via* method 2 are given in Figure 5 for the $[M(Ura\text{-}H)(H_2O)]^+$ ions. IR spectra for all optimized structures are compared to

the experimental fingerprint spectra for all ions in Figures S1 to S8, including those for both methods of computation.

Although no distinction could be made between the computed structures of Ba and Sr complexes in the 3200 – 3800 cm^{-1} region [14], enough evidence now exists to support definitive assignment of structure (i) as being the primary experimental structure for both ions, as is also the case for the Ca complex, although a hydrogen bonded O-H stretch is not experimentally observed. The feature in the area of 1610 – 1620 cm^{-1} (hydrogen bonded C=O stretching, H_2O scissoring and C5=C6 stretching combined modes) is more intense and broader than the one at 1510 cm^{-1} (metal coordinated carbonyl stretch). These two features are better reproduced by the calculated spectra of structure (i) in all three cases. Even more so, the small band observed at 1460 cm^{-1}, attributed to N1 hydrogen wagging, is matched in the calculated spectra for structure i, but absent in structure (ii) in all three cases. It is worth noting that for the complexes obtained with Ca, Sr and Ba, the shoulder experimentally observed on the blue side of the broad feature detected above 1610 cm^{-1} , is also quite well reproduced by the calculated spectra of N3O4/wb2 forms (i). In the stretch region, both the N-H stretch of uracil as well as the free O-H stretch of the water molecule in structure (i) of the Ca complex match well with the experimental spectra.

The experimental spectrum of the Mg complex only offers two distinct bands which may be used for assignment in the fingerprint region, while the O-H/N-H region offers more detailed information. The bands in the fingerprint regions correspond to the same predominant bands that are visible in the spectra for all other complexes – 1613 cm^{-1} for the hydrogen bonded C=O stretching, H_2O scissoring and C5=C6 stretching combined modes, and 1520 cm^{-1} for the metal coordinated carbonyl stretch. Both bands are prominently displayed in the calculated spectra for structures (i) and (iii). However, a lack of hydrogen bonding within the complex is suggested in

the experimental spectrum through the broad band centered about 3595 cm^{-1}. This would correlate more so with structure (iii), in which the symmetric and asymmetric stretches of water are plainly observed.

3.3. Computed structures for $[M(Ura-H)(H_2O)_2]^+$. A total of 7 isomers were obtained for the doubly-hydrated complexes of Ba, while 6 isomers we found for the complexes of Sr and Ca *via* method 1. Method 2 gives only 5 isomers for the Sr complex, the N3O2/wbO4/wbw structure obtaind with method 1 evolving towards the N3O2/wbO4/wbO2 when using method 2. There are 5 distinct isomers optimized for complexes of Mg through both methods. For both computational methods, the hypothesized Mg-N3O2/wbO4/wbw input collpases towards a Mg-N3O2/wbO4/w structure, similar to the behaviour of Sr. Figure 6 gives binding scheme and energetics for the three lowest energy structures. All structures obtained for both calculation methods are given in Figures S9 to S14 along with energetics, while Table summarizes the relative energies obtained with both calculations methods.

For each metal center, the N3O4/wbO2/wbO4 complex is the lowest energy forms in both enthalpy and Gibbs free energy. This result is consistent with previous findings obtained for the complexes of Ba and Sr [14]. In this structure, deprotonation occurs at the N3 of uracil, with metal coordination between N3 and O4, again confirmed by the presence of two BCPs of an electrostatic nature (positive values of $\nabla^2\rho$). Both water molecules are bound to the metal center, with an intramolecular hydrogen bond formed between one water molecule and O2, with the other water molecule forming an intermolecular hydrogen bond with O4. Note that in the case of both Ca and Mg, no hydrogen bonding is apparent between the water molecule and the O4 carbonyl (structures instead labelled as N3O4/wbO2/w). Consistently, the hydrogen bonds can be observed in the AIM

analysis for complexes of Ba and Sr, however no BCP is localized between the water molecule and O4 for the Ca or Mg complex. As already observed for the singly-hydrated complexes, the hydrogen bond length increases (and therefore their strength decreases), with decreasing the size of the metal ion. The hydrogen bond between water and O2 is far stronger than the hydrogen bond involving O4, presumably due to the fact that the O4 position is also the metal binding site. The carbonyl bond lengths are similar to those computed for singly-hydrated species, with the O2 carbonyl being shorter, ~1.24 Å, than the metal-coordinated O4 carbonyl, ~1.28 Å. Similar patterns are observed based on the size of the metal, though these trends are not as pronounced. As metal size increases, the metal-coordinated O4 carbonyl bond length decreases slightly. The length of the O2 carbonyl is the same for both the Ba and Sr complexes, and marginally shorter for the Ca complex.

The nearest isomer in terms of energy for the Sr and Ca complexes, which is at least 7.0 kJ mol^{-1} higher for all, is the N3O2/wbO4/wbO2 structure. The structure is very similar to the second lowest energy structure determined for singly-hydrated complexes, uracil being again deprotonated at the N3 position and metal coordination occuring between N3 and O2. Two water molecules are coordinated to the metal center, one being hydrogen-bonded to the O4 position and the other seemingly hydrogen-bonded to O2. However, the distance between the water molecule and O2 in the Ca complex suggests there is likely no interaction. Even so, the N3O2/wbO4/wbO2 label is still applied to this structure in order to differentiate this particular form and the structure (iii) (Fig. 6). For Ba, the N3O4/wbO2/wbw complex sits just slightly lower in energy. This structure takes the same conformation as the lowest energy singly-hydrated complex, with the additional water molecule bound between the metal center and the other water molecule. This complex does not represent a local energy minimuma for the other metals.

3.3.1. Comparison of computed and experimental spectra. A comparison between the experimental spectra and the three lowest energy structures computed *via* method 2 are given in Figure 7 for the $[M(Ura\text{-}H)(H_2O)_2]^+$ ions. Spectra for all optimized structures, based on both calculation methods, are compared to the experimental spectra for all ions in Figures S9 to S14. Good agreement is obtained in all cases between the experimental spectra and those calculated for structure (i). Previous studies could not distinguish between the doubly-hydrated structures of Ba and Sr in the 3200–3800 cm^{-1} region [14], but as was the case for the singly-solvated structures in this work, key features that are absent in the theoretical spectra for structures (ii) and (iii) allows structure (i) to be assigned to the observed ions.

Similar to the singly-hydrated species, the two prominent bands in the fingerprint regions give good agreement across all calculated spectra. The experimental bands in the area of 1620–1635 cm^{-1} (hydrogen-bonded C=O stretching, H_2O scissoring and C5=C6 stretching combined modes) as well as those at 1480–1530 cm^{-1} (metal-coordinated carbonyl stretch) agree well with the computed spectra for structure (i), especially for Sr and Ca (Figure 7). The feature centered at 1481 cm^{-1} for Ba is broader than the others and doesn't match as well with the spectrum for (i), as for Sr and Ca. The small band occurring between 1455 and 1480 cm^{-1}, which in the Ba spectrum appears as, at best, a shoulder to the red of the metal bound carbonyl stretch, is the result of N1 hydrogen wagging. The location of this vibration is only matched by the calculated spectra for structure (i) for each of the complexes.

As it was the case for the singly-hydrated species, both the N-H and free O-H stretches provide good agreement in the Ca and Mg complexes, however all computed lowest energy structures display exactly the same features. An N-H stretch is observed at 3475 cm^{-1} for

complexes of both metals. Two distinct free O-H stretching bands of water are found in the spectrum of the Mg complex, with both the asymmetric stretch as well as the free O-H stretch of the water hydrogen-bonded to uracil occurring at 3700 cm^{-1} and the symmetric stretch at 3630 cm^{-1}. Again, the lowest energy structure exhibits a strong hydrogen-bonded O-H band which is not observed in the experimental spectrum which prevents a definitive assignment of the experimental structure. For the Ca complex, similar O-H stretches are observed at 3700 cm^{-1} and 3640 cm^{-1}, as well as a seeming broad band below 3400 cm^{-1}, indicative of the hydrogen-bonded O-H stretch, further supporting structure (i) as the experimental structure of the Ca complex.

3.4. Computed structures for [Mg(Ura-H)(H$_2$O)$_3$]$^+$. Fifteen isomers of the triply-hydrated $[Mg(Ura-H)]^+$ ion were obtained through method 1. Of those, the five lowest energy structures were reoptimized using method 2. Figure 8 gives the structures and energetics for the three lowest energy structures, with all optimized structures given in Figure S17. Table S3 presents a comparison of thermochemistries deduced from both computational methods for the five lowest energy structures.

The lowest energy structure is deprotonated at the N3 position, with bidentate electrostatic Mg coordination to N3 and O4, as confirmed by AIM analysis. Three water molecules are all coordinated to the metal center, and are participating in hydrogen bonding with the uracil moiety – two water molecules presumably weakly interacting with O4 (though no localized BCPs are observed), and staggered on opposite sides of uracil, and the third water molecule hydrogen-bonded to O2 and found in the same plane as uracil. , . This particular structure is labelled as N3O4/2wbO4/wbO2 in Figure 8.

The O4 carbonyl, which participates to the metal coordination has a length of 1.280 Å; predictably shorter than the same carbonyl bond in the singly-hydrated complex (1.297 Å) and doubly-hydrated (1.286 Å). This shortening, and hence strengthening, of the carbonyl bond is attributed to the donation of electron density from the increased presence of water molecules weakening the M-O interaction, confirmed through AIM analysis by successively decreasing electron density at the BCPs as hydration increases. The O2 carbonyl length is 1.243 Å, which is only very slightly longer than the corresponding bond in the singly-hydrated (1.236 Å) and doubly-hydrated (1.240 Å) species. Both water-O4 hydrogen bonds measure ~2.85 Å, while the water-O2 hydrogen bond has a length of 1.764 Å.

The only other isomer computed to be close in energy to the lowest energy structure is N3O2/wbO4/2wbO2, which is located about 9 kJ mol^{-1} higher than N3O4/2wbO4/wbO2. In this particular isomer, deprotonation occurs at N3, with magnesium coordination now between N3 and O2. All three water molecules are again coordinated to magnesium. Two out of plane water molecules are hydrogen bonded to O2, while the third interact with O4 and lies in the same plane as uracil. The next lowest energy structure found is 35 kJ mol^{-1} higher than the global minimum.

3.4.1. Comparison of computed and experimental spectra. A comparison between the experimental spectra and the three lowest energy structures computed with method 2 are given in Figure 9 for the $[Mg(Ura\text{-}H)(H_2O)_3]^+$ ion. The five lowest energy structures, based on both calculation methods, are compared to the experimental spectra in Figures S18 and S19.

The agreement between the experimental IRMPD spectrum and the lowest energy structure is not bad although the most intense band is predicted to have a shoulder which is not observed. Structure iii also is in decent agreement although it is predicted to be considerably higher in energy.

The O2 carbonyl stretch, calculated for structure (i) to be at 1677 cm^{-1}, is visible in the experimental spectrum as a band of its own at 1681 cm^{-1}; the intense band centered about 1623 cm^{-1} is consistent with both scissoring of the water molecule hydrogen bonded to O2 (calculated at 1624 cm^{-1} for structure i) and the C5=C6 stretch (1615 cm^{-1} for structure i). The slight shoulder experimentally observed at 1590 cm^{-1} may be the result of synchronous (1592 cm^{-1}) and asynchronous (1588 cm^{-1}) scissoring of the out of plane water molecules, which may be isoenergetic with the most intense band in the experimental spectrum and could account for the higher than predicted intensity of this band. The scissoring motions of the two water molecules close to O4 in structure (iii) do not absorb with any appreciable intensity and are thus not observed in the calculated spectrum. A poor agreement between the spectrum of structure (ii) and the experimental trace is observed. Notably it cannot account for the two experimental bands detected at 1539 cm^{-1} and 1472 cm^{-1}. Both structure (i) and (iii) display the O4 carbonyl stretch at 1527 cm^{-1} and 1523 cm^{-1}, respectively, as well as N1 hydrogen wagging, computed at 1463 cm^{-1} for both.

The experimental spectra in the O-H/N-H region is nearly identical to that of the doubly-hydrated Mg complex – an N-H stretch at 3475 cm^{-1}, and two O-H stretches at 3720 and 3650 cm^{-1}, corresponding to the asymmetric and symmetric O-H stretches in water, respectively. All stretches are noticeably blue-shifted with increasing hydration. A feature at 3410 cm^{-1} does not correspond to any of the calculated structures and cannot be accounted for. As with the other complexes, a hydrogen bonded O-H stretch is not experimentally observed.

4. Summary

The structures of $[M(Ura\text{-}H)(H_2O)]^+$, where M corresponds to group 2 metal ions Ba^{2+}, Sr^{2+}, Ca^{2+} and Mg^{2+}, along with $[M(Ura\text{-}H)(H_2O)_2]^+$ for Ba^{2+}, Sr^{2+} and Ca^{2+} , as well as $[Mg(Ura\text{-}H)(H_2O)_3]^+$, were examined using IRMPD spectroscopy in the 1000–1900 cm^{-1} mid-infrared region. The same complexes were also examined in the 2700–3800 cm^{-1} O-H/N-H stretching region for Ca and Mg. Two different electronic structure calculation methods were employed for energy comparison of the various isomers, as well as for comparison to experimental spectra. There was good agreement between both computational methods for the structures, energies, and computed IR spectra. The IR spectra generated for these lowest energy structures also generally agreed best with the experimental IRMPD spectra.

For all complexes, the lowest energy structures are deprotonated at N3 of uracil with the metal bound by a bidentate electrostatic interaction with N3 and O4, confirmed through AIM analysis. Any water molecules present are bound to the metal ion, and participate in hydrogen bonding with the neighbouring carbonyls. In the case of a singly-hydrated complexes, a hydrogen bond between water and uracil is established at the O2 positon; for dehydrated ions, one water molecule is hydrogen bonded to O2 while the second one is hydrogen bonded to O4 (except for Ca and Mg, for which AIM analysis does not detect any water-O4 interaction). For the triply-hydrated Mg/uracil complex, , two water molecules are oriented toward O4, though no hydrogen bonds seem to be established, and the third water molecule is hydrogen bonded to O2.

For the complexes of Ba, Sr and Ca, only the lowest energy structure gave calculated spectra in suitable agreement with the experimental IRMPD spectra, and in each case the predominant contributor was easily assessed. For magnesium however, even if the spectra of the lowest energy isomer did provide suitable agreement, it could not be conclusively determined as the major contributor due to good spectral agreement from other isomers.

Acknowledgements

The authors wish to thank the CLIO team (J. M. Ortega, C. Six, G. Perilhous, J. P. Berthet) as well as P. Maître and V. Steinmetz for their support during the experiments. The authors also acknowledge the computational resources provided by ACE-Net and Westgrid. Finally, TDF acknowledges the financial contributions from NSERC, CFI, and Memorial University.

Figure Captions

Scheme 1. Numbering scheme for uracil.

Figure 1. IRMPD Spectra for $[Ba(Ura\text{-}H)(H_2O)]^+$, $[Sr(Ura\text{-}H)(H_2O)]^+$, $[Ca(Ura\text{-}H)(H_2O)]^+$ and $[Mg(Ura\text{-}H)(H_2O)]^+$ in the 1000–1900 cm^{-1} region.

Figure 2. IRMPD Spectra for $[Ba(Ura\text{-}H)(H_2O)_2]^+$, $[Sr(Ura\text{-}H)(H_2O)_2]^+$, $[Ca(Ura\text{-}H)(H_2O)_2]^+$ and $[Mg(Ura\text{-}H)(H_2O)_3]^+$ in the 1000–1900 cm^{-1} region.

Figure 3. IRMPD Spectra for $[Ca(Ura\text{-}H)(H_2O)_2]^+$, $[Ca(Ura\text{-}H)(H_2O)]^+$, $[Mg(Ura\text{-}H)(H_2O)_3]^+$, $[Mg(Ura\text{-}H)(H_2O)_2]^+$ and $[Mg(Ura\text{-}H)(H_2O)]^+$ in the 2700–3800 cm^{-1} region.

Figure 4. Comparison of the energies and structures for the three lowest energy $[M(Ura\text{-}H)(H_2O)]^+$ complexes, M=Ba, Sr, Ca, Mg. The thermochemistry reported here are those from method 2. Energies are expressed in $kJ.mol^{-1}$ and distances in Angströms.

Figure 5. Experimental IRMPD spectrum (bottom) for $[M(Ura\text{-}H)(H_2O)]^+$ compared with the B3LYP computed spectra using computational method 2 for the three lowest energy structures. Lowest energy structures represent the (i) N3O4/wbO2, (ii) N3O2/wbO4 and (iii) N3O4/wbO4 tautomers. The relative enthalpies and Gibbs free energies (italics) calculated at 298 K are also shown in $kJ.mol^{-1}$.

Figure 6. Comparison of the energies and structures for the three lowest energy [M(Ura-H)$(H_2O)_2]^+$ complexes, M=Ba, Sr, Ca, Mg. The thermochemistry reported here are those from method 2. Energies are expressed in kJ.mol^{-1} and distances in Angströms.

Figure 7. Experimental IRMPD spectrum (bottom) for [M(Ura-H)$(H_2O)_2]^+$ compared with the B3LYP computed spectra using computational method 2 for the three lowest energy structures. Lowest energy structures represent the (i) N3O4/wbO2/w(bO4), (ii) N3O2/wbO4/w(bO2) and (iii) N3O2/wbO4/w tautomers. The relative enthalpies and Gibbs free energies (italics) calculated at 298 K are also shown in kJ.mol^{-1}.

Figure 8. Comparison of the energies and structures for the three lowest energy [Mg(Ura-H)(Ura)$(H_2O)_3]^+$ complexes. The thermochemistry reported here are those from method 2. Energies are expressed in kJ.mol^{-1} and distances in Angströms.

Figure 9. Experimental IRMPD spectrum (bottom) for [Mg(Ura-H)$(H_2O)_3]^+$ compared with the B3LYP computed spectra using computational method 2 for the three lowest energy structures. Lowest energy structures represent the (i) N3O4/2wbO4/wbO2, (ii) N3O2/wbO4/2wbO2 and (iii) N3O4/wbO2/wbwbO4 tautomers. The relative enthalpies and Gibbs free energies (italics) calculated at 298 K are also shown in kJ.mol^{-1}.

References

[1] A.M. Pyle, Science, 261 (1993) 709.

[2] D.L. Nelson, M.M. Cox, Lehninger, Principles of Biochemistry, third ed., W.H. Freeman, New York, NY, 2004 (Chapter 10).

[3] G.L. Eichhorn, L.G. Marzilli, Advances in Inorganic Biochemistry: Metal Ions in Genetic Information Transfer vol. 3, Elsevier Science, New York, NY, 1981, pp. 1.

[4] P.-O. Lowdin, Rev. Mod. Phys., 35 (1963) 724.

[5] P.O.P. Ts'o, Basic Principles in Nucleic Acids Chemistry, Academic Press, New York, NY, 1974.

[6] M.D. Topal, J.R. Fresco, Nature, 263 (1976) 285.

[7] H. Ruterjans, E. Kaun, W.E. Hull, H.H. Limbach, Nucleic Acid Res., 10 (1982) 7.

[8] K. Nakanishi, N. Suzuki, F. Yamazaki, Bull. Chem. Soc. Jpn., 34 (1961) 53.

[9] M.A. Kurinovich, J.K. Lee, J. Am. Chem. Soc., 122 (2000) 6258.

[10] T.M. Miller, S.T. Arnold, A.A. Viggiano, A.E. Stevens Miller, J. Phys. Chem. A, 108 (2004) 3439.

[11] M.T. Nguyen, A.K. Chandra, T. Zeegers-Huyskens, J. Chem. Soc., Faraday Trans., 94 (1998) 1277.

[12] Y. Huang, H. Kenttamaa, J. Phys. Chem. A, 107 (2003) 4893.

[13] S.M. Bachrach, M.W. Dzierlenga, J. Phys. Chem. A, 115 (2011) 5674.

[14] A.A. Power, O.Y. Ali, M.B. Burt, T.D. Fridgen, Int. J. Mass Spectrom., 330–332 (2012) 233.

[15] B. Power, V. Haldys, J.-Y. Salpin, T.D. Fridgen, Int. J. Mass Spectrom., 378 (2015) 328.

[16] O.Y. Ali, N.M. Randell, T. D. Fridgen, ChemPhysChem, 13 (2012) 1507.

[17] T.D. Fridgen, Mass Spectrom. Rev., 28 (2009) 586.

[18] N.C. Polfer, J. Oomens, Mass Spectrom. Rev., 28 (2009) 468.

[19] R. Prazeres, F. Glotin, C. Insa, D. A. Jaroszynski, J. M. Ortega, Eur. Phys. J. D, 3 (1998) 87.

[20] W. Paul, Rev. Mod. Phys., 62 (1990) 531.

[21] K. Rajabi, M. L. Easterling, T. D. Fridgen, J. Am. Soc. Mass Spectrom., 20 (2009) 411.

[22] M. Azargun, T.D. Fridgen, Phys. Chem. Chem. Phys., (2015) http://dx.doi.org/10.1039/C5CP00580A

[23] Gaussian 09, Revision D.01, M.J. Frisch, G.W. Trucks, H.B. Schlegel, G.E. Scuseria, M.A. Robb, J.R. Cheeseman, G. Scalmani, V. Barone, B. Mennucci, G.A. Petersson, H. Nakatsuji, M. Caricato, X. Li, H.P. Hratchian, A.F. Izmaylov, J. Bloino, G. Zheng, J.L. Sonnenberg, M. Hada, M. Ehara, K. Toyota, R. Fukuda, J. Hasegawa, M. Ishida, T. Nakajima, Y. Honda, O. Kitao, H. Nakai, T. Vreven, J.A. Montgomery, Jr., J.E. Peralta, F. Ogliaro, M. Bearpark, J.J. Heyd, E. Brothers, K.N. Kudin, V.N. Staroverov, T. Keith, R. Kobayashi, J. Normand, K. Raghavachari, A. Rendell, J.C. Burant, S.S. Iyengar, J. Tomasi, M. Cossi, N. Rega, J.M. Millam, M. Klene, J.E. Knox, J.B. Cross, V. Bakken, C. Adamo, J. Jaramillo, R. Gomperts, R.E. Stratmann, O. Yazyev, A.J. Austin, R. Cammi, C. Pomelli, J.W. Ochterski, R.L. Martin, K. Morokuma, V.G. Zakrzewski, G.A. Voth, P.

Salvador, J.J. Dannenberg, S. Dapprich, A.D. Daniels, O. Farkas, J.B. Foresman, J.V. Ortiz, J. Cioslowski, D.J. Fox, Gaussian, Inc., Wallingford CT, (2013).
[24] P.B. Armentrout, M. Citir, Y. Chen, M.T. Rodgers, J. Phys. Chem. A, 116 (2012) 11823.
[25] P.B. Armentrout, Y. Chen, M.T. Rodgers, J. Phys. Chem. A, 116 (2012) 3989.
[26] R. F. W. Bader, Atoms in molecules: a quantum theory, Clarendon Press ; Oxford University Press, Oxford, New York, 1990.
[27] AIMAll (Version 14.10.27), Todd A. Keith, TK Gristmill Software, Overland Park KS, USA, 2014 (aim.tkgristmill.com)
[28] O.Y. Ali, T.D. Fridgen, Int. J. Mass Spectrom., 308 (2011) 167.
[29] P. Colarusso, K. Zhang, B. Gup, P.F. Bernath, Chem Phys Lett, 269 (1997) 39.
[30] Y.-w. Nei, T.E. Akinyemi, C.M. Kaczan, J.D. Steill, G. Berden, J. Oomens, M.T. Rodgers, Int. J. Mass Spectrom., 308 (2011) 191.

Scheme 1.

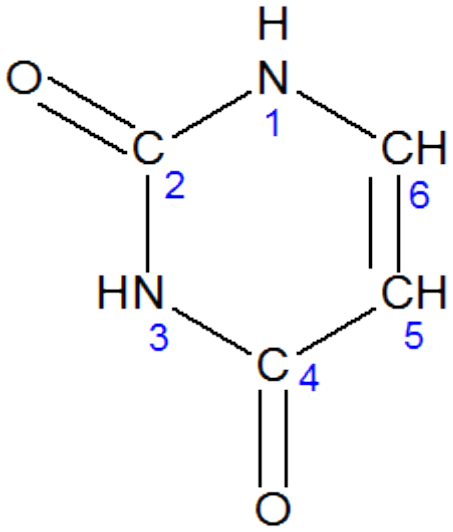

Figure 1.

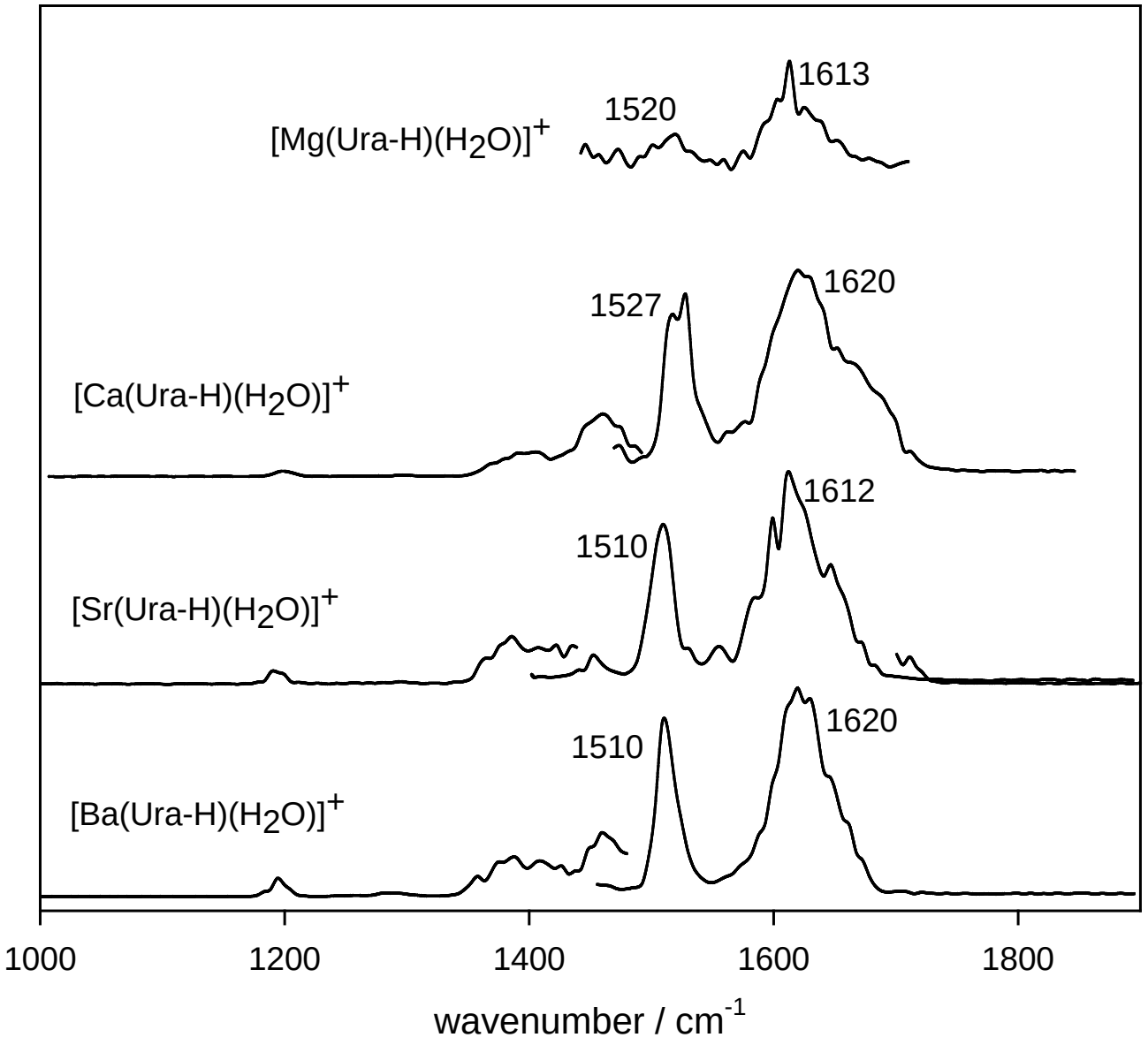
[Mg(Ura-H)(H2O)]+
1520
1613
[Ca(Ura-H)(H2O)]+
1527
1620
[Sr(Ura-H)(H2O)]+
1510
1612
[Ba(Ura-H)(H2O)]+
1510
1620
1000
1200
1400
1600
1800
wavenumber / cm-1

Figure 2.

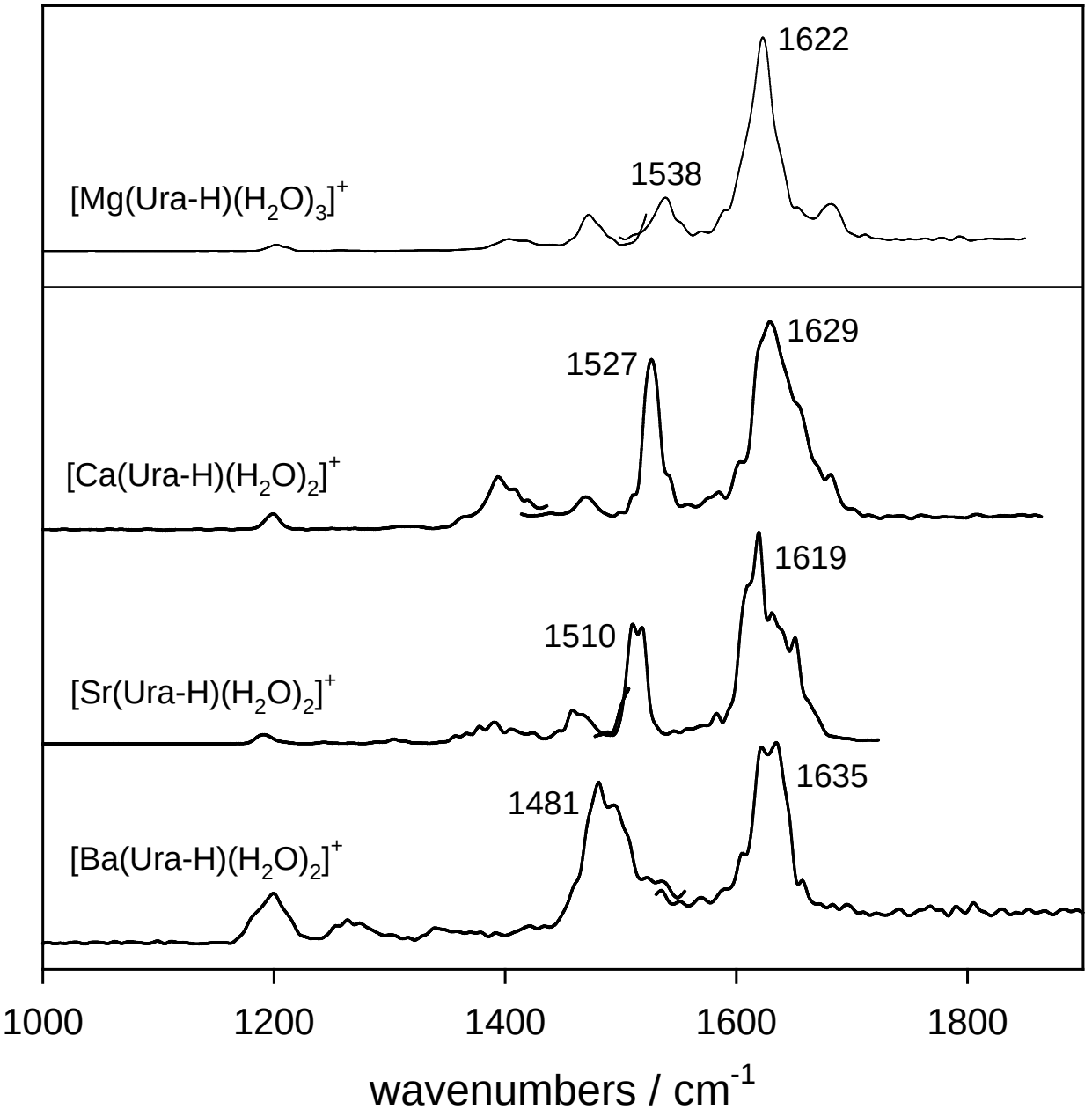
1622
1538
[Mg(Ura-H)(H2O)3]+
1629
1527
[Ca(Ura-H)(H2O)2]+
1619
1510
[Sr(Ura-H)(H2O)2]+
1635
1481
[Ba(Ura-H)(H2O)2]+
1000
1200
1400
1600
1800
wavenumbers / cm-1

Figure 3.

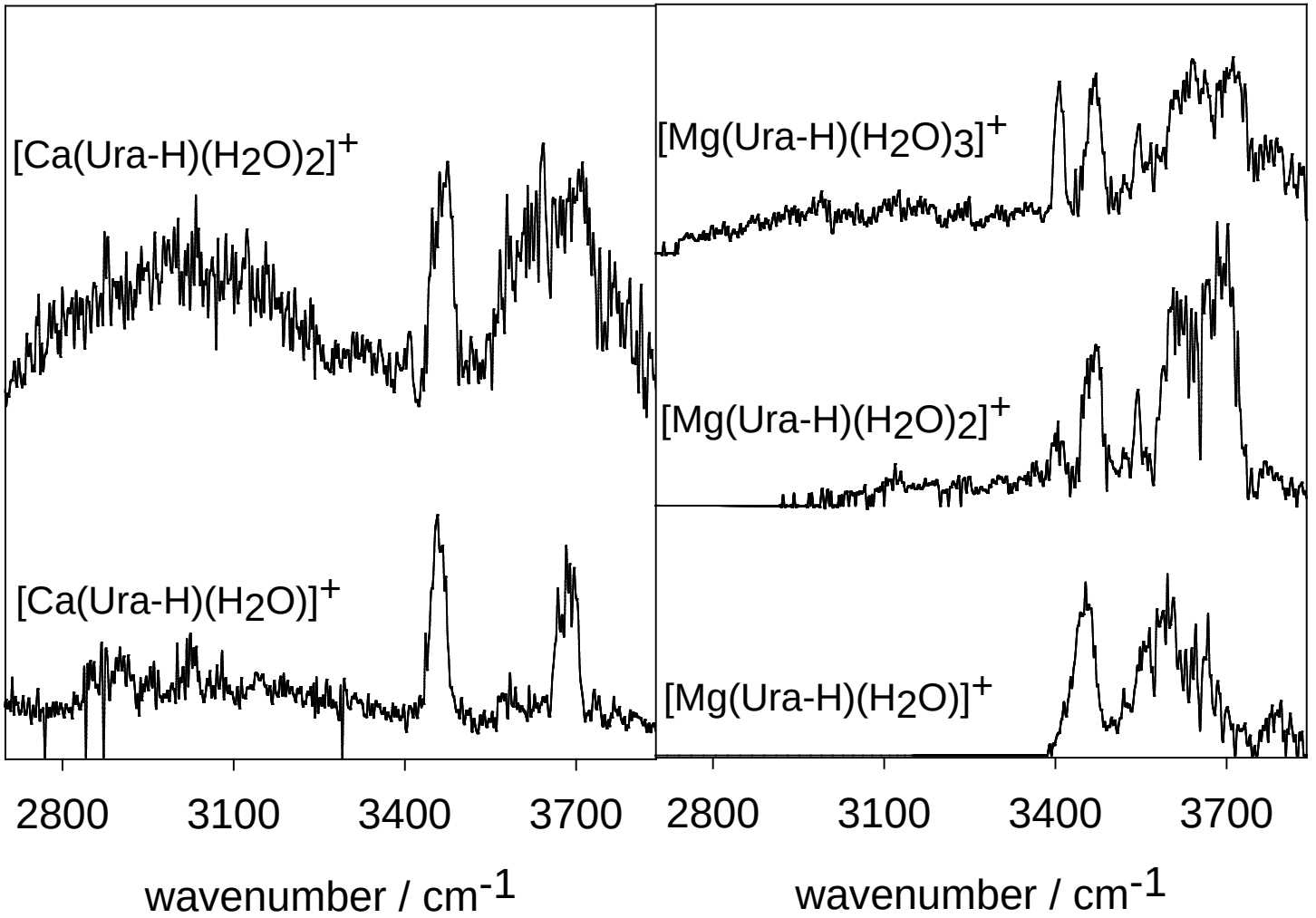
[Ca(Ura-H)(H2O)2]+
[Ca(Ura-H)(H2O)]+
[Mg(Ura-H)(H2O)3]+
[Mg(Ura-H)(H2O)2]+
[Mg(Ura-H)(H2O)]+
2800
3100
3400
3700
2800
3100
3400
3700
wavenumber / cm-1
wavenumber / cm-1

Figure 4.

iii

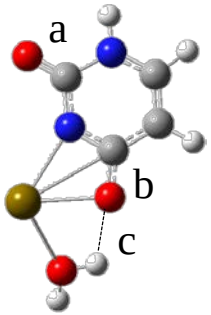

Ba,Sr,Ca-N3O4/wbO4
Mg-N3O4/w

M	$\Delta_{rel}H/\Delta_{rel}G$	a	b	c
Ba	39.6/*34.4*	1.225	1.293	2.074
Sr	39.3/*33.0*	1.223	1.296	2.264
Ca	35.1/*23.6*	1.221	1.299	3.577
Mg	1.2/*0*	1.217	1.301	n/a

ii

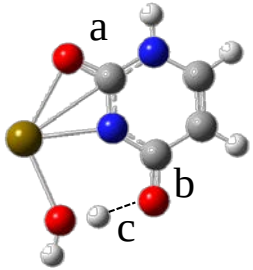

M-N3O2/wbO4

M	$\Delta_{rel}H/\Delta_{rel}G$	a	b	c
Ba	5.6/*5.8*	1.273	1.251	1.549
Sr	6.1/*6.3*	1.275	1.251	1.556
Ca	6.9/*7.1*	1.278	1.249	1.580
Mg	13.1/*16.7*	1.290	1.245	1.737

i

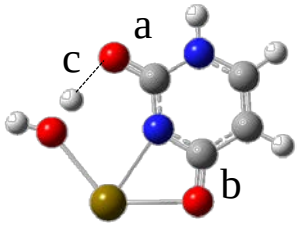

M-N3O4/wbO2

M	$\Delta_{rel}H/\Delta_{rel}G$	a	b	c
Ba	0/*0*	1.246	1.279	1.619
Sr	0/*0*	1.245	1.281	1.638
Ca	0/*0*	1.243	1.285	1.673
Mg	0/*5.6*	1.236	1.297	1.942

Figure 5.

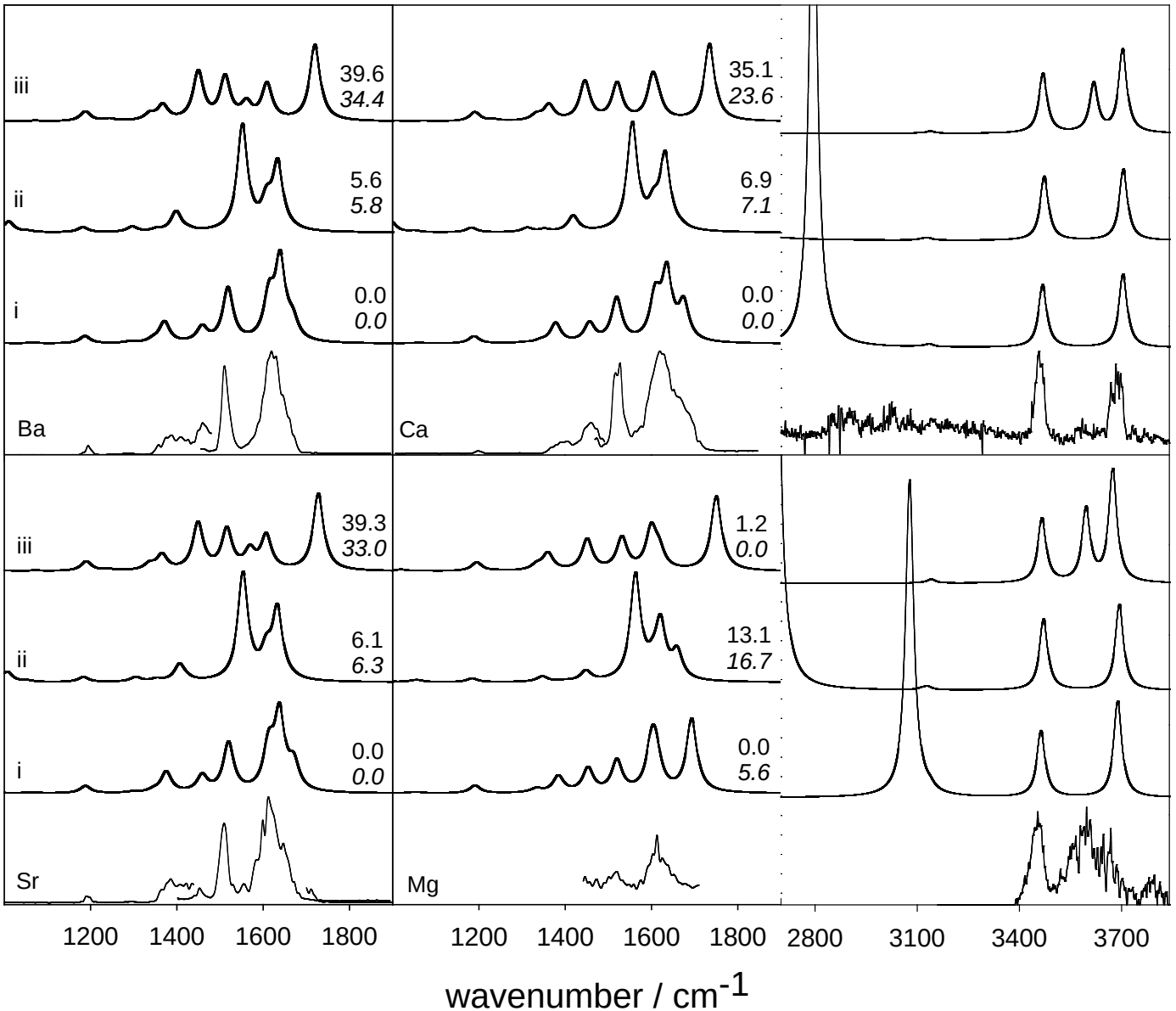
iii
39.6
34.4
ii
5.6
5.8
i
0.0
0.0
Ba
Ca
35.1
23.6
6.9
7.1
0.0
0.0
iii
39.3
33.0
ii
6.1
6.3
i
0.0
0.0
Sr
Mg
1.2
0.0
13.1
16.7
0.0
5.6
1200
1400
1600
1800
2800
3100
3400
3700
wavenumber / cm-1

Figure 6.

iii

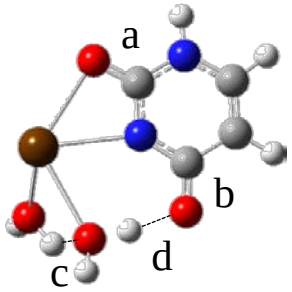

Ba-N3O2/wbO4/wbw
Ca-N3O2/wbO4/w

M	$\Delta_{rel}H/\Delta_{rel}G$	a	b	c	d
Ba	10.3/*11.2*	1.270	1.255	2.201	1.525
Ca	14.6/*9.2*	1.275	1.252	4.640	1.597

ii

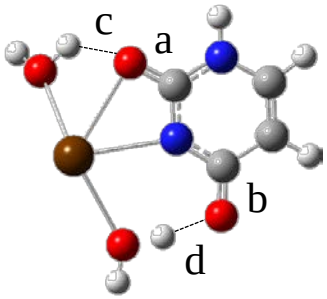

Ba,Sr,Ca-N3O2/wbO4/wbO2
Mg-N3O2/wbO4/w

M	$\Delta_{rel}H/\Delta_{rel}G$	a	b	c	d
Ba	7.0/*7.0*	1.274	1.251	2.061	1.559
Sr	7.1/*7.2*	1.275	1.251	2.186	1.567
Ca	7.5/*7.2*	1.276	1.250	2.417	1.586
Mg	10.5/*10.2*	1.279	1.247	3.004	1.667

i

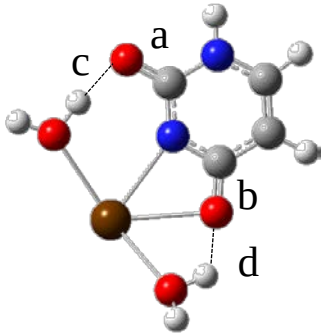

Ba,Sr-N3O4/wbO2/wbO4
Ca,Mg-N3O4/wbO2/w

M	$\Delta_{rel}H/\Delta_{rel}G$	a	b	c	d
Ba	0/*0*	1.246	1.280	1.629	2.048
Sr	0/*0*	1.246	1.281	1.644	2.166
Ca	0/*0*	1.244	1.283	1.675	2.359
Mg	0/*0*	1.240	1.286	1.802	2.982

Figure 7.

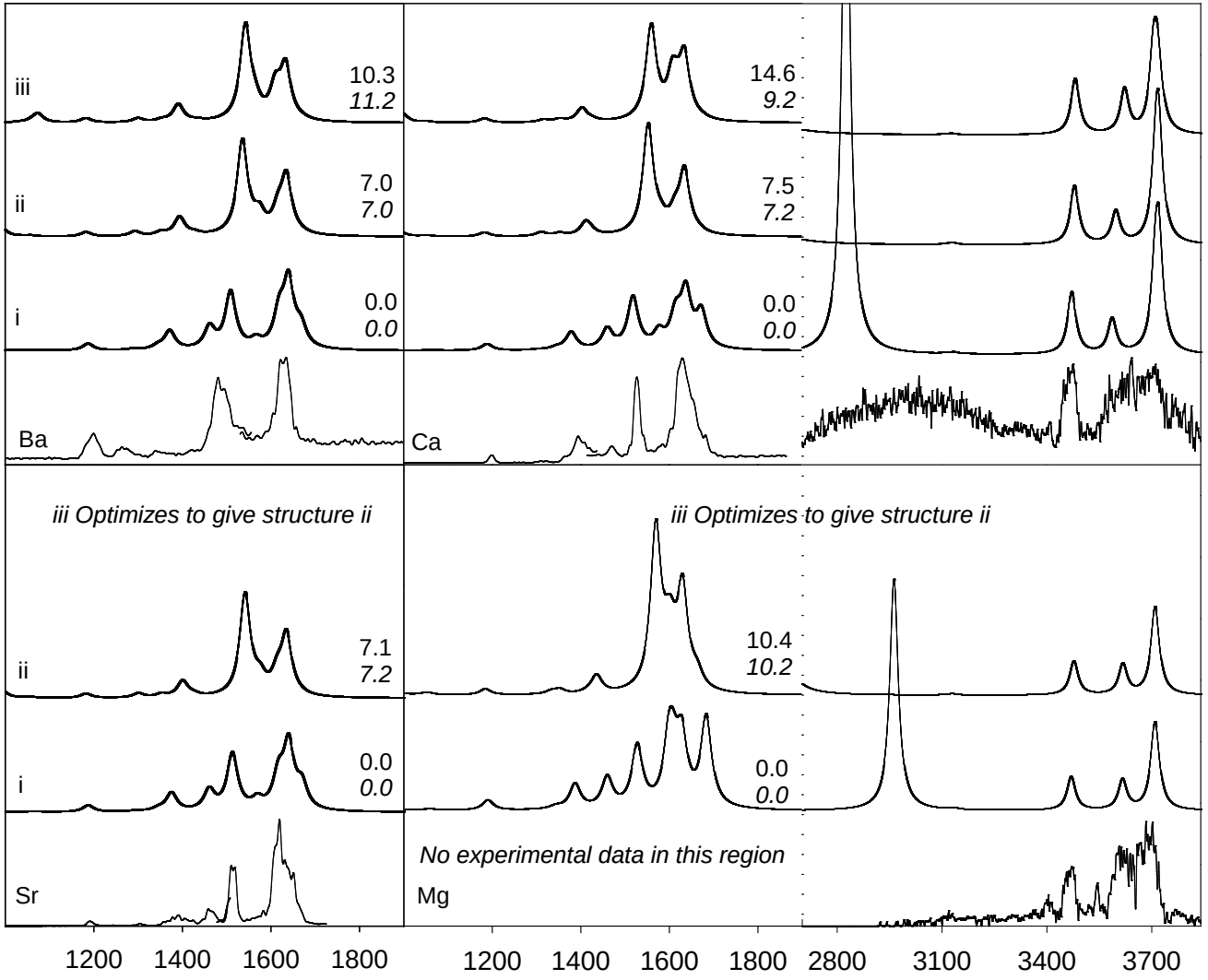
iii
10.3
11.2
ii
7.0
7.0
i
0.0
0.0
Ba
Ca
14.6
9.2
7.5
7.2
0.0
0.0
iii Optimizes to give structure ii
iii Optimizes to give structure ii
ii
7.1
7.2
i
0.0
0.0
Sr
Mg
10.4
10.2
0.0
0.0
No experimental data in this region
1200
1400
1600
1800
1200
1400
1600
1800
2800
3100
3400
3700
wavenumber / cm-1

Figure 8.

iii

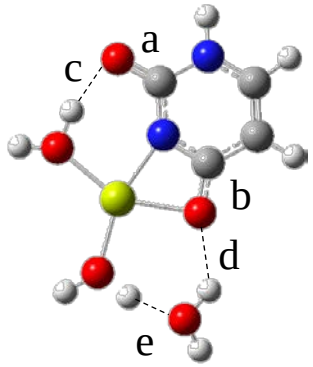

$\Delta_{rel}H/\Delta_{rel}G$	a	b	c	d	e
35.2/*42.8*	1.239	1.287	1.787	2.011	1.545

ii

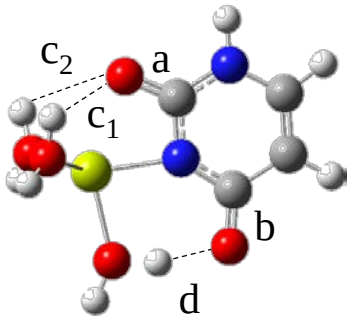

$\Delta_{rel}H/\Delta_{rel}G$	a	b	c_1	c_2	d
9.0/*9.9*	1.272	1.250	2.759	2.984	1.628

i

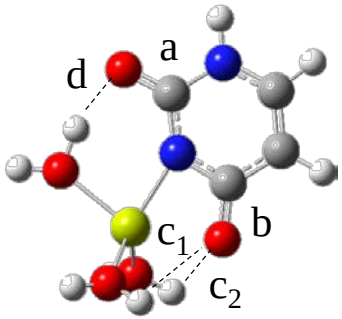

$\Delta_{rel}H/\Delta_{rel}G$	a	b	c_1	c_2	d
0/*0*	1.243	1.281	2.851	2.858	1.764

Figure 9.

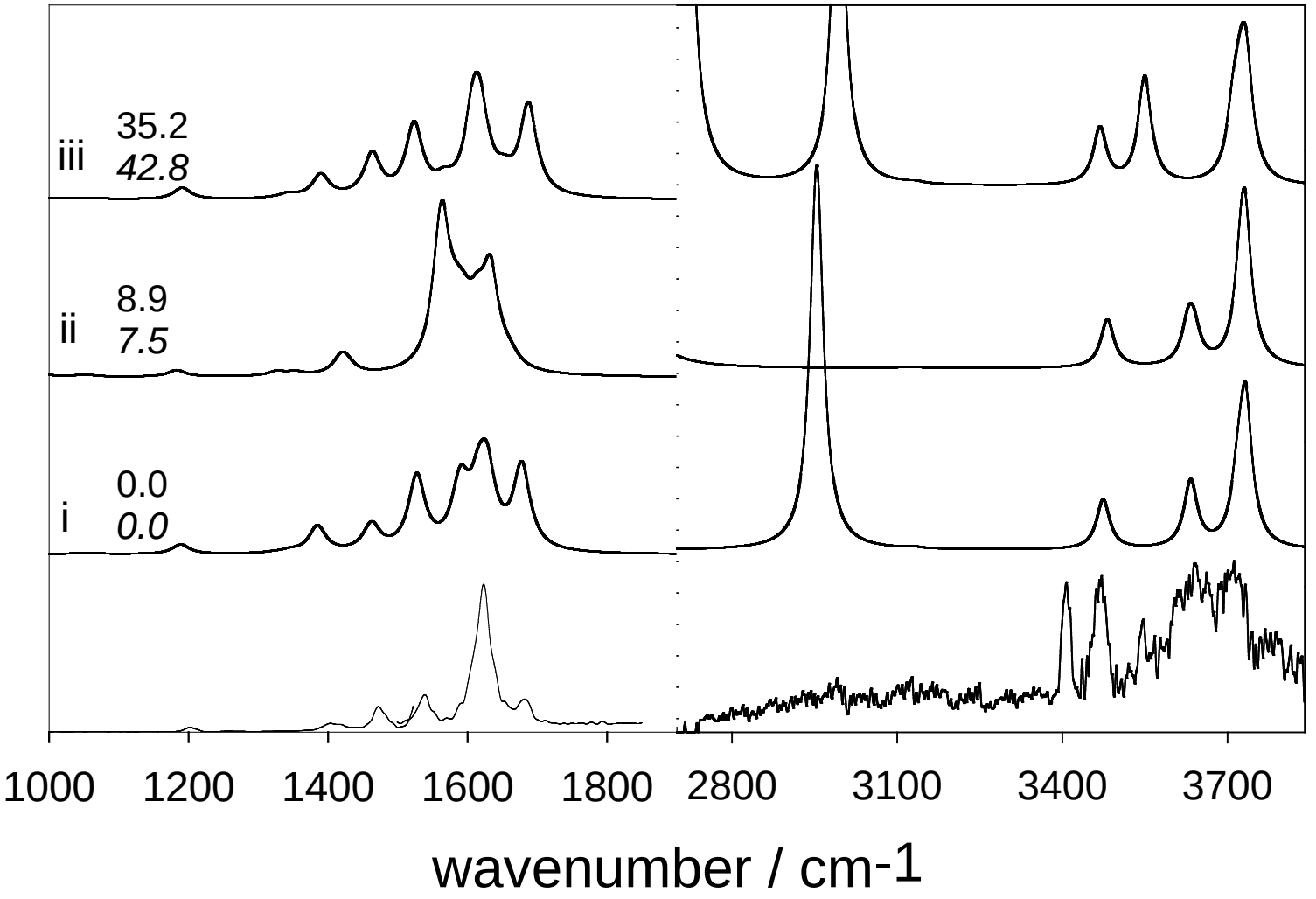
iii
35.2
42.8
ii
8.9
7.5
i
0.0
0.0
1000
1200
1400
1600
1800
2800
3100
3400
3700
wavenumber / cm-1